Oligodendrocyte Tethering Effect on Hyperelastic 3D Response of Axons in White Matter

Mohit Agarwal, Parameshwaran Pasupathy, Assimina A. Pelegri *

Mechanical and Aerospace Engineering Rutgers University-New Brunswick, Piscataway, NJ 08854, USA

Abstract

A novel finite element model is proposed to study the mechanical response of axons embedded in extracellular matrix when subjected to tensile loads under purely non-affine kinematic boundary conditions. Ogden hyperelastic material model describes the axons and the extracellular matrix material characterizations. Two axon-glia tethering scenarios in white matter are studied a single oligodendrocyte (single-OL) with multiple connections a multi-oligodendrocyte (multi-OL) one. In the multi-OL tethering configuration, resultant forces are randomly oriented as distributed glial cells arbitrarily wrap around axons in their immediate vicinity. In the single-OL setup, a centrally located oligodendrocyte myelinates multiple axons nearby. Tethering forces are directed towards this oligodendrocyte, resulting in greater directionality and farther-reaching stress distribution. The oligodendrocyte connections to axons are represented by a spring-dashpot model. The material properties of myelin served as the upper limit for the parameterization of the oligodendrocyte stiffness ("K"). The proposed FE models enable realization of connection mechanisms and their influence on axonal stiffness to determine resultant stress states accurately. Root mean square deviation analysis of stress-strain plots of different connection scenarios reveal an increasing axonal stiffness with increasing tethering, indicating the role of oligodendrocytes in stress redistribution. In single-OL submodel, for the same number of connections per axons, RMSD values increased as "K" (the oligodendrocyte spring stiffness) values were set higher. RMSD calculations reveal that for a "K" value, single-OL model yielded slightly stiffer models compared to multi-OL. The current study also addresses the potential geometrical limitations of multi-OL model by randomizing and adding connections to ensure greater responsiveness. Cyclic bending stresses noticed in both submodels suggest the risk of axonal damage accumulation and repeated load failure.

Keywords: micromechanics, finite elements, oligodendrocyte, axonal injury, CNS white matter, multi-scale simulation, hyperelastic materials, Abaqus

Nomenclature

 α alpha

 μ shear moduli (hyperelastic: Ogden model)

 λ principal stretches σ principal stress

K spring-dashpot stiffness

1

^{*} Corresponding author, pelegri@rutgers.edu

1. Introduction

Traumatic Brain Injury (TBI) is one of the most researched topics of the 21st century and a significant global public health problem. Traumatic brain injury (TBI) can be defined as an acquired insult to the brain from an external mechanical force that could result in temporary or permanent impairment [1-3]. TBI has been reported as the leading cause of death and disability among children and young adults in the United States. It is estimated that 1.5 million Americans sustain a TBI annually [4], while at least 10 million severe enough TBI cases occur annually [4]. Moderate to severe TBIs can have long-lasting or permanent effects such as cerebrovascular damage, neuronal deformation, hypoxia, cerebral edema, and increased intracranial pressure [5].

In recent years, the number of TBI diagnoses has increased rapidly. However, efforts to accurately measure and predict cerebral injury have been a major challenge. The corpus callosum has been identified as a critical region for TBI, with axonal injury being the proximal cause [6-10]. Axonal damage has been identified as the leading cause of TBI, with excessive tensile strain postulated as the underlying mechanism [6]. The use of finite element (FE) methods to predict and understand axonal injury has yielded significant breakthroughs. An inverse FE method to predict material properties of the axons by matching experimental data with simulations was first proposed by Pan et al. [11-13]. Yousefsani et al. developed an FE model using the embedded element technique to bind axons of varying diameters to the extracellular matrix (ECM) when subjected to transverse loading [14]. Karami et al. used a fiber-reinforced composite model to represent an axon following a sinusoidal path embedded in the ECM and subject to bending, tension, and shear [15]. The above studies use affine boundary conditions which tie the axon entirely to the ECM. Nevertheless, axon tortuosity depends on stretch and consecutively axons exhibit a "transitional" behavior from non-affine at a low stretch to affine at high stretch values when tortuosity decreases [13]. The mechanical response of embedded axons to external loads is also influenced by glial cells that wrap axons with myelin. Glial cells insulate axons and facilitate tethering among nearby axons.

Oligodendrocytes are specialized glial cells that myelinate the axons in the gray and white matter of the central nervous system (Figure 1). The mechanical response of myelinated axons was previously investigated by *Shreiber et al.* [16, 17]. The results show that myelination improves the stiffness of the axons. However, since a single oligodendrocyte may connect to 80 axons [18, 19] it is hypothesized that the stress-strain response of the axon/glial composite tissue is affected by the spatial oligodendrocyte/axon network. To this end a model is developed to probe the tethering effect of the oligodendrocytes. The model incorporates a purely non-affine boundary condition between the axons and the ECM. The methods employed and the results obtained are presented here.

Brainstem and corpus callosum if subjected to high strains or high strain rates are susceptible to severe axonal damage [7, 20-22]. Through these studies, it was concluded that stiffness and anisotropic response of the brainstem coupled with its location as a narrow bridge between CNS regions contributed to its compounded vulnerability. Brain tissues show significant variations in overall material stiffness, and critical regions have anisotropic material properties, which ultimately contribute to larger local deformations on the vulnerable sites. Ever-increasing computational capabilities have enabled generating high-fidelity models of the microstructure of

the brain. FEM for computational analysis of TBI dates back to the early 1970s (2D – FE models), while 3D FEM models burst onto the scene during the 1990s [23-26]. To date, a universal material model characterizing brain tissues has not been categorically identified, thus underlying the vast scope of improvement in the field of FEM-based TBI modeling. Over the past decade, a broad spectrum of axonal material models has emerged, ranging from linear elastic [27, 28], viscoelastic to sophisticated hyperelastic material models to define properties for brain soft matter [23, 29-34]. Specifically, Montanino et al. [29-31] have conducted multiscale studies using both whole head and micromechanics FE models. In their latest work, they integrated molecular dynamics simulation in their model to obtain mechanoporation thresholds aiming to infer axonal damage. Their model assumes cylindrical, non-undulated axons embedded in a glial matrix, and is subject specific. The work presented here includes the inherent tortuosity of the axons that contributes to the reversal of stresses manifested in repeated loads [2]. The proposed FEM could enable depiction of resultant bending stresses that could arise when micro-FE model is subjected to tensile loads and possible cyclic failure.

Moreover, hybrid techniques such as inverse finite element analysis to predict axonal material properties have also been proposed to identify material parameters to closest approximations [11-13]. TBI researchers have devoted significant effort to identifying optimal FE model geometry [15, 23, 35-37] and interfacing parameters between the axons and ECM to mimic actual stress transfer when subjected to traumatic loads [13, 14, 38, 39]. Some of the early work in the field assumed affine boundary conditions to model the axons and ECMs whereby the axons are entirely tied down to the ECM [11, 14, 15]. These approximations can be further improved by incorporating the transitional behavior manifested by the axon and the glia as a function of stretch/strain and axonal tortuosity [2, 13].

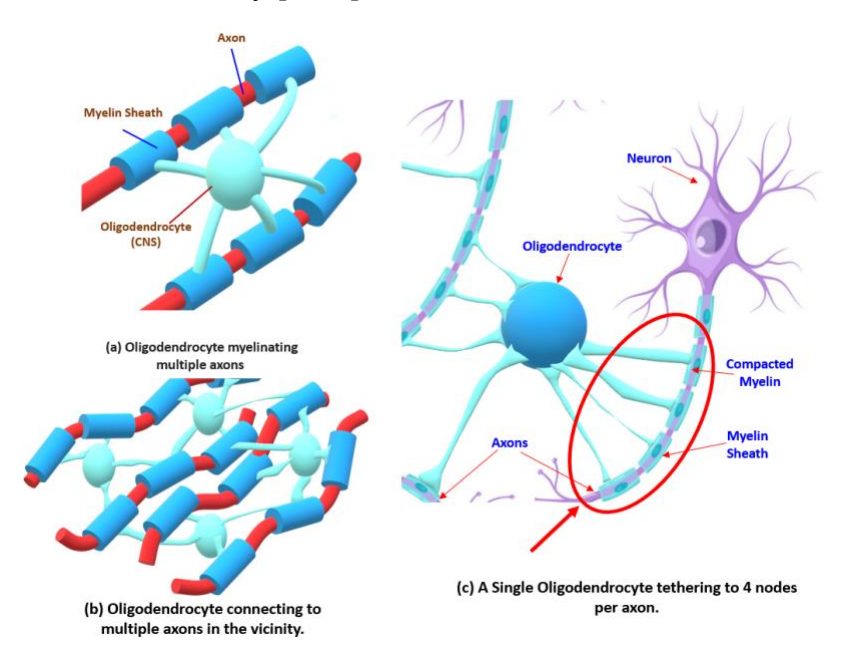


FIGURE 1: (a) Oligodendrocyte facilitating myelination in multiple axons in its vicinity. (b) 3D schematic of multiple oligodendrocyte connections with nearby axons. (c) Single oligodendrocyte connecting at multiple nodes (4 -nodes in the labeled zone) per axon.

In this study, a novel FEM is proposed that allows oligodendrocytes to wrap around the outer diameter of axons to depict this physiological tethering. The oligodendrocyte connections to axons are represented by a spring-dashpot model[2, 3]. Such a connection model mimics the tethering between oligodendrocytes and axons, facilitating inter-axonal bonding and creating a myelin sheath that insulates and supports axons in the brainstem. The FE model aims to mimic two dominant tethering configurations in brain white matter (multi-OL: Figure 1b and single-OL: Figure 1a). Thus, two FE submodels are put forward: 1) multiple oligodendrocytes arbitrarily tethered to the nearest axons (multi-OL model), and 2) single oligodendrocyte tethered to all axons at various locations (single-OL model). A proof-of-concept FE model is improved and analyzed to probe the effect of the tethering by the oligodendrocytes for an ensemble of connection scenarios. The proposed FE models would help depict axonal mechanical response and estimate extent of axonal injuries. This research will also serve as reference for future full-scale computational models to evaluate axonal repeated load and damage accumulation.

2. Computational Model Development

Oligodendrocytes produce myelin which wraps around the axons, insulate, and facilitate tethering amongst adjacent axons. Oligodendrocytes' bonding mechanisms and higher stiffness of myelinated axons are described in [2, 3]. Glial cells provide mechanical support to embedded axons and dictate the response of the axons to tensile loading [8, 16, 17]. The glial cells create a scaffold that supports the axons and bind 80 axons to a single oligodendrocyte. Oligodendrocyte tethering in brain white matter could take place in two ways. First, in a multi-oligo tethering configuration, where resultant forces are randomly oriented, distributed oligodendrocytes arbitrarily wrap around axons in their immediate vicinity. Second, via single-oligo configuration, in which oligodendrocyte stationed centrally, simultaneously myelinates multiple axons nearby. Resultant tethering forces directing towards this oligodendrocyte result in greater directionality and farreaching stress distribution [3, 40]. Thus, spatial arrangement dictates resultant tethering force directions.

The influence of myelination on axonal stiffness is well recorded [8, 41], nevertheless, the impact of varying tethering from oligodendrocytes on the mechanical response of axons is still at its fledgling stage. The current study investigates the effect of oligodendrocyte tethering on axon's mechanical response by simulating an ensemble of connection scenarios for two models (see Figures 2a, 2c) outlined in later sections. In total, two (2) independent sets of simulations (for two FE submodels) are performed for brain matter, and mechanical response trends of multi-OL and single-OL models are analyzed in §3.2 and §3.3, respectively. Comparative analyses are carried out to determine relative stiffness variations for different cases in the ensemble (see §3.4). The same spring-dashpot approximation [2] is used to model the arms of the oligodendrocyte that tether to the axons.

A distributed coupling constraint is used to model the nucleus [2, 3]. Since the scope of the study is limited to characterizing the mechanical response of the arms of the oligodendrocyte and not the nucleus itself, the nucleus is modeled as a distributed coupling constraint in Abaqus [41]. Such a model constrains the "coupling nodes" motion to the reference node's translation and rotation, allowing for the distribution of loads through a weighting factor between the reference and the

coupling nodes based on a user-specified influence radius. Here, the oligodendrocyte is visualized as a sphere of $0.025~\mu m$ embedded inside the ECM.

The microscale FEMs are developed with Abaqus 2020 and Python scripting. The representative elemental volume (REV) for modeling axons tethered to glia in CNS white matter is based on the FE models developed by $Pan\ et\ al.$ [2, 11]. Axons of varying undulation and radii are embedded in a 3D rectangular ECM with dimensions: $x = 0.9\ \mu m$, $y = 8\ \mu m$, $z = 5.747\ \mu m$. Undulation varies from axon to axon based on the work by $Bain\ et\ al.$ [8], with average undulation varying from 1.00 to 1.10 [42, 43]. The axons' diameter varies from a minimum of 0.4 μ m to a maximum of 0.62 μ m with an average axonal diameter of 0.45 μ m. Following the same setup as used in previous work (see [2, 3] for more details on FEM setup), non-affine boundary conditions between the axons and ECM are established using a "surface to surface" contact definition (see Figure 1 [3]) [41]. The axon-ECM contact identified to be frictionless in the tangential direction. Hard contact defined in the normal direction [41]. The ECM here chosen as the master surface and the axons as the slave surface [40]. Note, that in Abaqus a hard contact condition minimizes the penetration of surfaces at and impedes tensile stress across the constrained interface [41].

In Figure 2, oligodendrocytes of $0.025~\mu m$ radius are inserted in the ECM [40]. The reference node of the distributed coupling is located at the center of the sphere. The nodes of the ECM along the surface of the sphere act as coupling nodes (coupling constraints and contact definition used in the FEM model can be found in [2, 40]). The influence radius is set to the radius of the sphere with a uniform weighting method and a weight factor of 1 [2, 3].

To the best of our knowledge, there is no reported data which characterizes the viscous behavior of the oligodendrocytes. In proposed FEM, simulation uses a ramping method to apply the load, where Abaqus linearly increments the load for each time step. Therefore, in order to accommodate the viscous behavior, a dashpot with a small dashpot coefficient of 1 kg/s is included. A linear spring-dashpot [3, 40] connects different points along the length of the axon to the center of the oligodendrocyte sphere, as shown in Figure 2(b) and Figure 3. The spring and dashpot are connected in parallel, using a spring rate of 10 N/m and a damping coefficient of 1 kg/s [40]. Spring-dashpot tool in Abaqus assigns a linear element representative of spring and dashpot in parallel [3, 40, 41]. For the ensemble of cases, the spring-dashpot values are parametrically varied to depict various tethering scenarios (see §3.2).

This paper utilizes the Ogden hyperelastic material model to simulate the ECM and the axons [2]. Non-linear hyperelastic models are commonly used to simulate soft biological tissues [11, 13, 23, 35]. Some of the pioneering work in the field including Ogden hyperelastic material model from *Pan et al.* [11-13], *Karami et al.* [15] and *Mihai et al.* [44] referred to formulate hyperelastic material model for this study [2, 40]. The non-linearity of the Ogden model allows neural tissue to be characterized more accurately for large deformation and strains. The Ogden hyperelastic model is based on the three principal stretches λ_1 , λ_2 , λ_3 , and 2N material constants. The strain energy density function, W, for the Ogden material model (Equation A.1) in Abaqus is formulated as [2, 41] and it is detailed in Appendix A. The incompressible, single parameter Ogden hyperelastic material model and principal stress constitutive equations are also explained in Appendix A (Equation A.2 and Equation A.3).

The oligodendrocyte material properties used for the Ogden hyperelastic model are $\mu_o = 32.8$ kPa, $\alpha = 8.22$ [17, 40]. This material was modeled as incompressible [2, 40]. This explanation is also added to the note in the Appendix A for reader's reference.

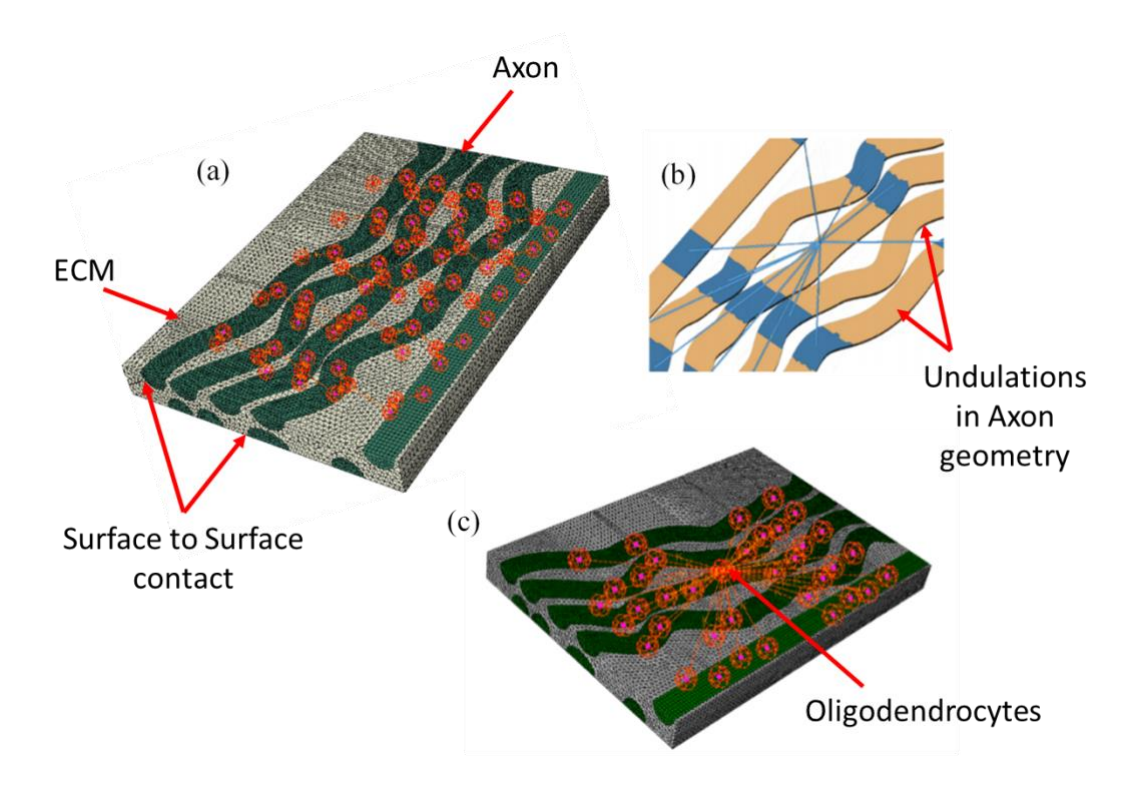


FIGURE 2: (a) Multi-OL model: Oligodendrocytes arbitrarily tethered to axons, (b) a schematic representation of an oligodendrocyte tethering to axons at different locations via a sheath of myelin, (c) Single-OL model: single oligodendrocyte tethering to surrounding axons [3].

2.1. Finite Element models

In the current study, the two submodels presented previously [2, 3] are further improved to study the effect of oligodendrocyte tethering on axons' mechanical response. For the first submodel (multi-OL case), a plane between the axon layers is created with 25 grid points equally spaced (see [2, 3] for FEM geometrical configuration details). In the second submodel (single-OL case), a single oligodendrocyte ties to all the axons embedded at different sites. The sole oligodendrocyte is positioned at the center of the ECM (see Figure 2c). In this paper, connections between axons and oligodendrocytes are further parameterized to complete the ensemble and gain perspective on the mechanical response for each connection configuration (see Figure 3). As outlined before, spring-dashpot elements simulate the tethering arms of the oligodendrocyte in the proposed FEM [2]. Upon literature review, no published literature sources were found which could characterize oligodendrocyte stiffness. Hence, the axons' stress-strain response was obtained by parametric variation of spring-dashpot connection ('K'). The material properties of myelin served as the upper limit during parameterization of oligodendrocytes stiffness.

The model uses symmetric boundary conditions on the top, and bottom faces in x-coordinate direction and side faces in y-coordinate direction. Constraints are applied in the z-direction using fixed boundary conditions (B.C.) on one face, and a stretch is applied to the opposite face using non-zero displacement boundary conditions (see Figure 3f). An implicit time integration solver technique is used in Abaqus for computation. Contact stabilization prevents rigid body modes before contact is established between interacting surfaces of the axons and ECM [2]. In total, the new finite element mesh consisted of 84,209 nodes with 359,707elements. 355,509elements were tetrahedral of type C3D4H, 3648 hexahedral elements of type C3D8H, and 342 wedge elements of C3D6H were generated on the model geometries. All elements required a linear hybrid formulation due to the hyperelastic material assignment [2, 40, 45].

The geometrical variations and parameterization schema deployed in this study followed the distribution of axon oligodendrocyte connections provided by literature data [18, 19] (also discussed in §1) in which the values were acquired through microtome of CNS white matter [40]. Two FE models are proposed; a multiple oligodendrocytes array arbitrarily tethered to the nearest axons (referred to as **multi-oligodendrocyte or multi-OLs**), and 2) a single oligodendrocyte tethered to all the axons at various locations (referred as **single-oligodendrocyte or single-OL**). These two models intend to capture variations in mechanical response that may arise from each of these tethering arrangements (discussed later in Figures 13 and 14). Both sets of results depicted stiffening of the axons, indicate that oligodendrocytes aid in redistributing stress and mechanical response. Note that in previous work, multi-OL model is referred as submodel-1 and single-OL model is mentioned as submodel-2. Refer to [2, 3] for more information.

Table 1: Material properties of FE submodels

Component	μ MPa	<i>D</i> 1/ MPa	α	Element Type
Axon	2.15E-03	0	6.19	C3D8H C3D4H
ECM	8.5 E-04	0	6.19	C3D4H

The mechanical properties of the axon and glia are assumed from previous work and literature data [2, 29, 35, 46]. In this study, the values for shear modulus for the axons and glial are obtained from research by Wu et al. [46] while α is derived from the model developed by Meaney [35]. The shear modulus of the ECM is assigned relative to the shear modulus of the axon, considering axons are three times stiffer than ECM, as reported by Arbogast and Margulies [7]. Refer to Table 1 for summary of material properties and element definition used in the FE model. From a parametrization point of view, the FE model developed in this study can be analyzed with a wide range of material properties. The strain energy density function would simply scale corresponding to the input material properties.

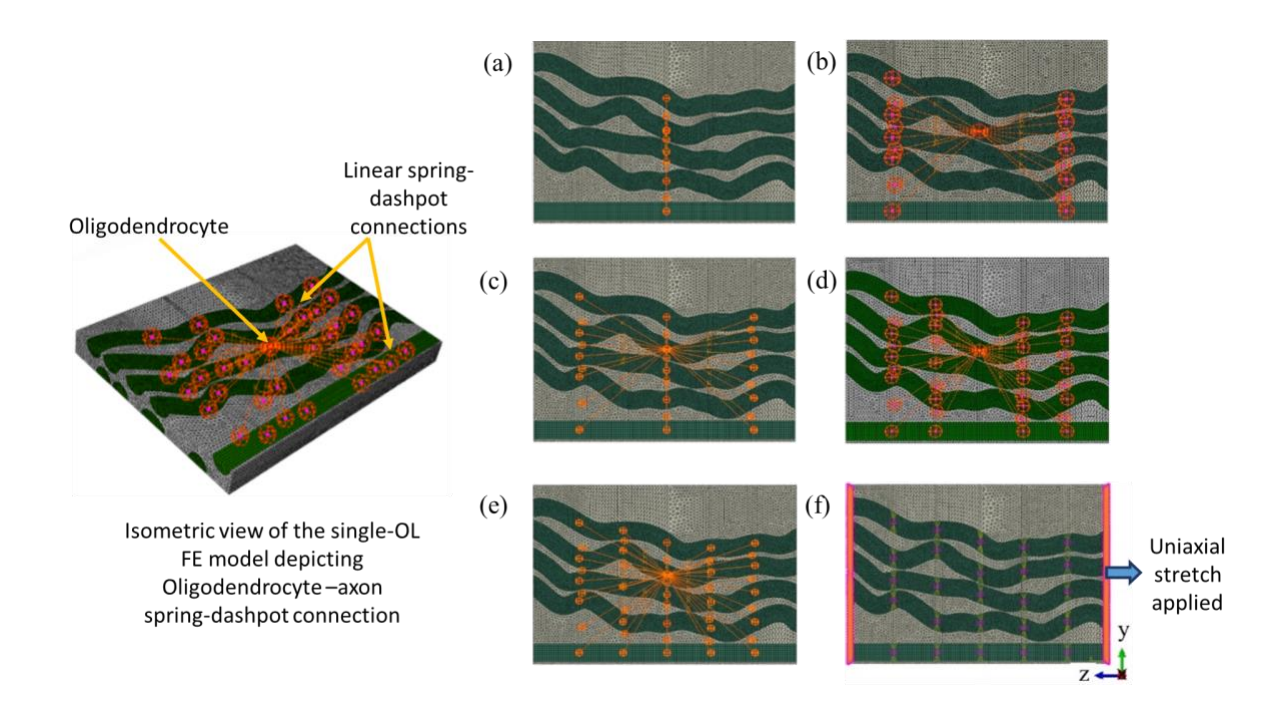


FIGURE 3: (a-e) Parameterization of the number of connections between oligodendrocyte and each axon in single-OL model showing 1, 2, 3, 4, and 5 connections per axon, (f) boundary conditions for the FE model with the left end fixed and a stretch applied on the right [3].

2.2. Multi-OL FE model Setups & Boundary conditions

Initial multi-OL setup : As discussed before, a plane between the axon layers is created for the first submodel (termed the multi-OL model in this paper), and 25 grid points are evenly spaced [2]. The oligodendrocyte nucleus is generated as a sphere with a radius of $0.025~\mu m$ at each point. These oligodendrocyte spheres are attached to any axon connection point within a radius of $0.05~\mu m$ via a spring-dashpot connection. The maximum number of axons connected to a single oligodendrocyte is four (4), with some oligodendrocytes only connecting to one axon (see Figure 4a).

Revised multi-OL FE setup: The results reported in [2] and [3] showed that the variation in mechanical response was indistinguishable even with varying oligodendrocyte arm stiffness (*K*). This stemmed out due to an inherent geometrical constraint in multi-OL model, i.e., all connections between the oligodendrocytes and the axons are in xy-plane and perpendicular to z-direction. As the model deforms (stretches along the z-axis), the springs did not experience any net deformation along the z-axis. This would have been the primary direction that stiffened the axonal mechanical response. This issue is overcome by incorporating additional interplanar connections along the z-direction. Results and observations have been listed in §3.2 and §3.3. Due to the additional connections, the maximum number of axons connected to a single oligodendrocyte is six (6), with some oligodendrocytes only connecting to two axons (see Figure 4b).

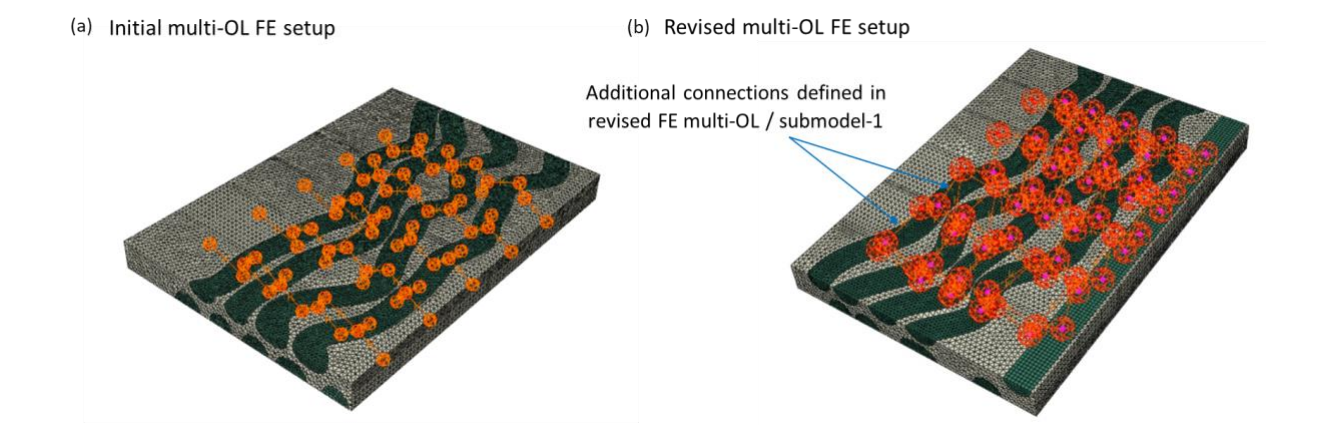


FIGURE 4: (a) Initial multi-OL model: Oligodendrocytes arbitrarily tethered to axons. This FE configuration denoted as the multi-OL model or SM1 in this study interchangeably. In the original multi-OL FE setup, total of 69 connections is incorporated. (b) Revised multi-OL model: Oligodendrocytes arbitrarily tethered to axons in and out of the plane. In total, 120 connections are present in the revised multi-OL model.

Table 2: Summary of the FE submodels and their nomenclature in current and previous work.

S.No.	FE Model Type	FE model variants / sub-types explored	Nomenclature for FEM	
1	multi-oligodendrocyte or	Initial multi-OL setup (Total 69 connections)	Submodel-1[2, 3]	
2	multi-Ols FEM	Revised multi-OL FE setup (Total 120 connections)	Introduced in this paper.	
		Total 5 cases explored for varying connections		
3 s	single-oligodendrocyte or single-OL FEM	1 node per axon (9conn)	Submodel-2[2, 3]	
		2 nodes per axon (18conn)		
		3 nodes per axon (27conn)		
		4 nodes per axon (36conn)		
		5 nodes per axon (45conn)		

Table 2 outlines FE-submodels discussed along with their nomelcature for ease of the reader. These submodels were also parametrically evaluated for varying spring stiffness 'K' values of 10, 50, 75 and 100 N/m. Results and discussions on each ensemble case follows in later sections.

3. Results and Discussion

3.1. Multi-OL model

For the present analysis, the micromechanical FE model is subjected to uniaxial stretch in the z-direction. As a representative case, FEM contour plots results for revised multi-OL (120 connections) and single-OL (5 nodes per axon and total 9 axons in model = 45 connections) FE ensemble cases are plotted side by side. For the chosen models, a stress profile is reported for the

20% stretch case in the z-direction. Similar stress contour plots as in [2] were obtained. As reported previously, tortuosity prevents full extensions in axons (see Figure 5 and Figure 6) [47].

As shown in Figure 5, the straight axon is in full tension while the undulated axons experience bending stresses along their tortuous path (see [2] for the effect of bending stress). These bending stresses tend to undergo cyclic reversal from tension to compression at each inflection point along the length of axon as seen in Figure 6. The presence of bending stresses increases the risk of damage accumulation and repeated load failure [2, 48, 49]. Due to revisions on multi-OL, von-Misses stress values are comparable with the single-oligodendrocyte model (see Figures 5 and 6) [2]. Even though current results do not account for any cumulative damages on axonal injuries, numerical results obtained using the axon-ECM FE material model may serve as a reference for any future study related to full-scale repeated load analysis.

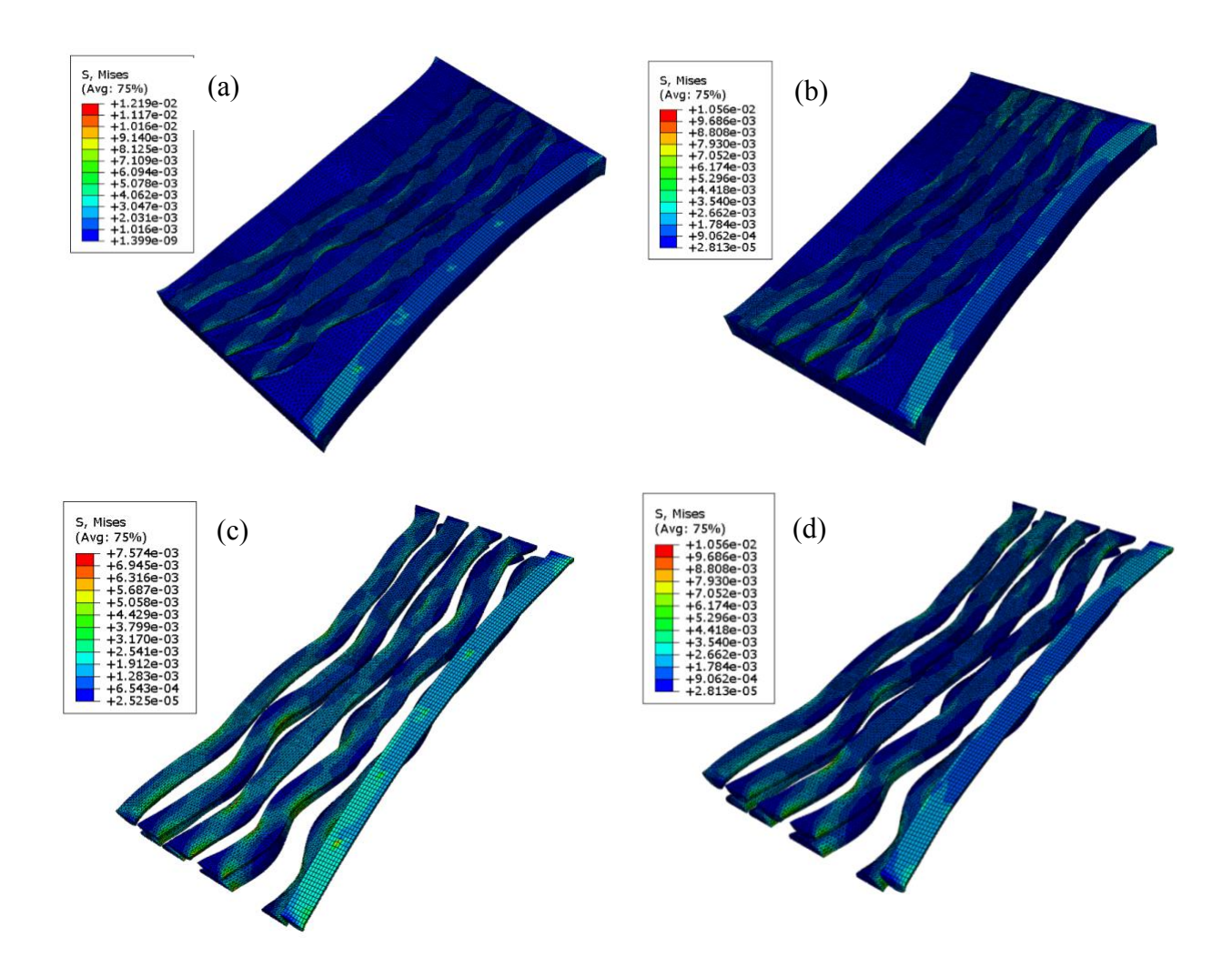


FIGURE 5: Von Mises stress contour for the ECM (a-b) and the axons (c-d) at 20% applied to stretch for: (a),(c) revised multi-OL (total 120 connections) and (b),(d) 5-nodes per axon (single-OL) FE micro-mechanical models. Both cases also observed the undulation of axons resulting in a high stress in the concave regions.

As discussed in §2.2, multi-OL contains a total of 25 oligodendrocyte spheres tethering to the nearest axons (total 69 connections). In the current study, the revised multi-OL version (refer to §2.2) overcomes some of the potential geometrical limitations of the original multi-OL model [2, 3]. In the revised multi-OL model, random additional spring-dashpot tethering (120 connections) have been introduced along the direction of stretch (z-axis), and the mechanical response is evaluated (Figure 5a). On the other hand, single-OL model contains a single oligodendrocyte at the FE model center tethered to all the axons. For single-OL model, the number of connections was parametrically varied to further investigate variations in stiffness for the entire ensemble. Note for clarity: multi-OL FE model is termed as submodel-1 and single-OL FE model termed as submodel-2 in our previous research papers ([2, 3]).

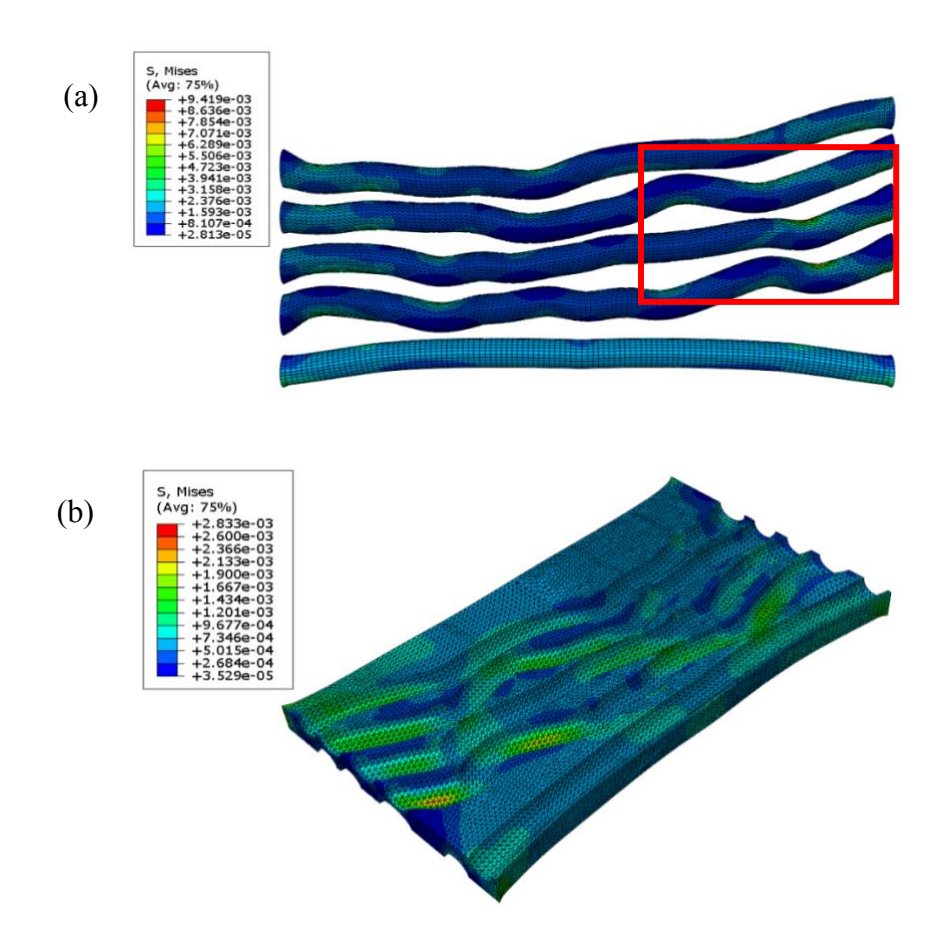


FIGURE 6: (a) Bending stresses undergoing complete reversal (see marked rectangular region) from tension to compression for FE-micromechanical with axon & ECM material properties (b) Von-Mises stress contour plot exclusive for ECM

3.2. Analysis on multi-OL FE models

Multi-OL (69conn) FE model

The stress-strain behavior for the original multi-OL FE model (total 69 connections) is computed by varying spring-dashpot stiffness. The spring-dashpot connection is parameterized for different

stiffness values. K = 10, 50, 75 and 100 N/m. In order to circumvent the lack of experimental data for oligodendrocyte stiffness, the model employs the RVE geometry and the ECM material properties to determine the spring stiffness, and to simulate different tethering cases. Our fundamental premise is that the oligodendrocyte tethering is an extension of the ECM. Given this assumption, a plausible approach was to consider the material properties of the ECM itself as an upper limit to motivate the properties of the spring constant for the oligodendrocyte tethering. To achieve this, we considered the scenario that the ECM is treated as a spring itself.

To present the significance of these stiffness values (K) from a physiological context, K = 10 N/m represents a tethering connection that is 30 times weaker than the ECM [3]. From applied force viewpoint, this parametric variation can be described as causing a net 10% strain (i.e., 0.568 μ m), the minimum load required would vary in the ratio 1:5:10 for 10K: 50K: 100K stiffness models (denoting 10 N/m as 10K and so forth). These stiffnesses are much lower than traditional macrocomponent level springs, but in context of brain matter strain energy variations, they bring significant variations in the micromechanical FE model.

<u>Multi-OL (120conn)</u> FE model

between curves for varying K values also stayed the same.

In the case of the revised multi-OL FE model with 120 connections, stress-strain behavior for varying spring-dashpot stiffness (K) was performed by solving up to 80% (4x) longitudinal strain (see Figure 7). The spring-dashpot connection is parameterized for different stiffness values. K = 10, 50, 75 and 100 N/m. Figure 7 indicates that the stiffness of revised multi-OL model is only marginally stiffer (Root Mean Square Deviation, RMSD [2]: 0.00019 at 10K), although the model gets progressively stiffer (RMSD: 0.00194 at 100K). Here, RMSD (is defined as $\sqrt{\sum \frac{(f(x_i) - g(x_i)^2}{N}}$ for curves f(x), g(x) and N being number of points x_i at which curves are compared. In fact, for 10K model, at lower strains (below 26.5%), 69conn_multi-OL model was observed to be stiffer than the revised 120conn_ multi-OL model. Thus, introducing inter-planar connection in the z-direction led to a minor increase in mechanical stiffness response. Moreover, the relative trends

Comparing revised 120conn_multi-OL with single-OL model, RMSD value for the two submodels with K=10 N/m is 0.00158, with K=75 N/m RMSD is 0.00478, and with K=100 N/m RMSD increases to 0.00482 (see Figure 11). Inclusion of additional connections in multi-OL model proved to be stiffer than single-OL FE model at K=10 N/m, while the RMSD values between the corresponding curves reduced compared to results reported previously [3]. This strongly indicates that introducing additional connections in z-direction yields a more responsive multi-OL FE model.

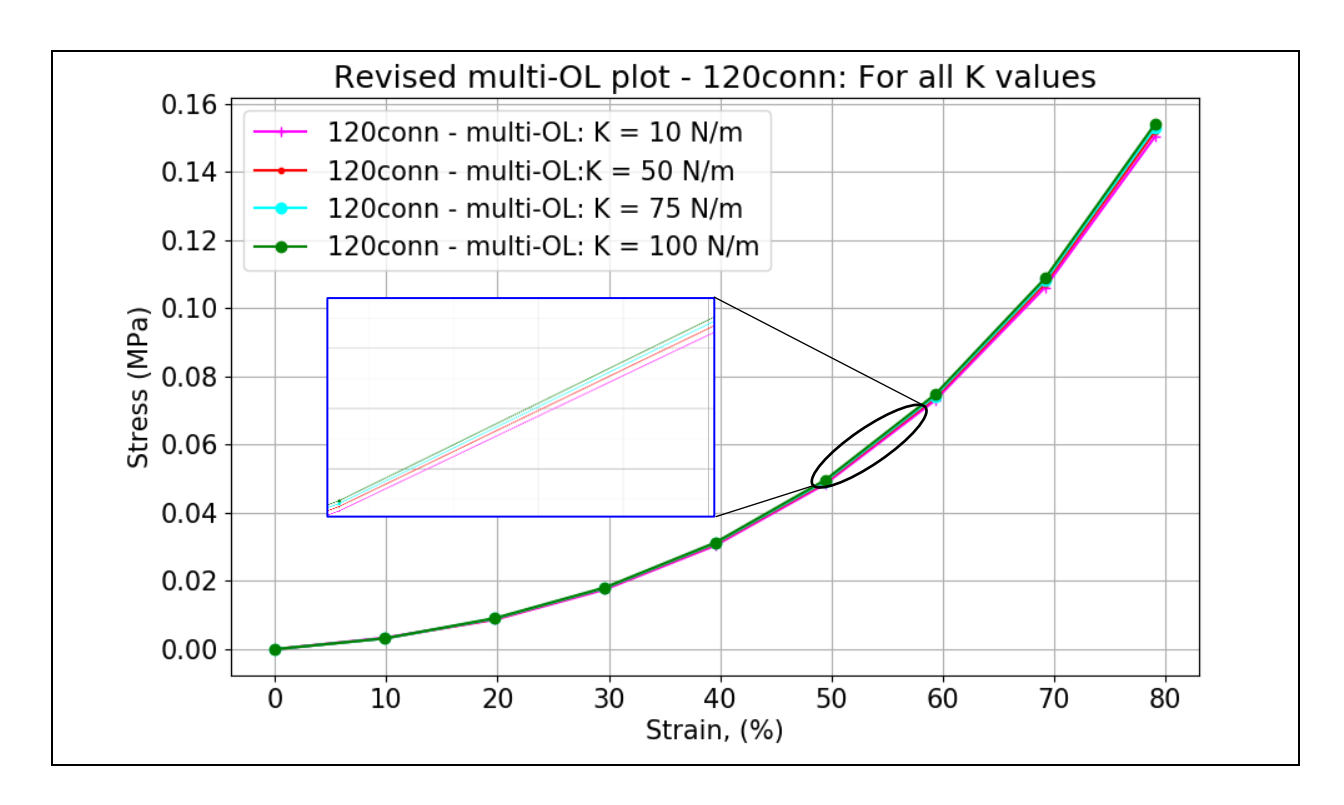


FIGURE 7: Combined Stress (σ) versus stretch plot for revised multi-OL (120 connections) for varying spring-dashpot stiffness (K) parameters, solving up to 80% strain. multi-OL model shows marginal variation in mechanical response with varying K.

Performance comparison between multi-OL versions

Due to additional connections in multi-OL model, the maximum stress observed at 80% stretch was higher than the stress in the 69conn_multi-OL model discussed in [2] and [3]. While increasing connections does not substantially alter the mechanical response in revised multi-OL model at lower K values (0.25% increase at K =10 N/m case), the maximum stress rose by 2.73% at higher K values (K = 100 N/m). The RMSD values also indicate significant variation with increasing K values (see Figure 8). RMSD differences among the K-dependent curves are (10K and 50K curves) < (10K and 75K curves) < (10K and 100K curves), see Table 3.

Table 3: RMSD analysis for varying K values in the revised multi-OL FE model plots

RMSD Comparison Chart (multi-OL model: Revised setup)			
Plots compared	RMSD Value		
10 <i>K</i> and 50 <i>K</i>	0.00072		
10 <i>K</i> and 75 <i>K</i>	0.00122		
10 <i>K</i> and 100 <i>K</i>	0.00169		

As shown in Table 3, a significant increase in model stiffness is noticed at K = 100 N/m for revised multi-OL model. On the other hand, for original multi-OL model (69 connections), RMSD value between 10K and 100K curves were calculated to be 0.00015. Thus, revised multi-OL model is stiffer at higher K values due to added interplanar connections. Thus, geometrical modifications in the multi-OL FE model helped overcome the indistinguishability limitations reported in [3]. The revised multi-OL model results suggest that oligodendrocytes play a vital role in increasing axons' stiffness and mechanical response in both submodels (multi- and single-OL setups).

Table 4: Original and revised multi-OL FEM stiffness comparison for corresponding K values

RMSD Comparison Chart (multi-OL FEM: Original vs. Revised) for corresponding K values			
Plots compared	K value	RMSD Value	
(0	10 <i>K</i>	0.0001880	
69conn_multi-OL and 120conn_multi-OL	50 <i>K</i>	0.0016906	
	75 <i>K</i>	0.0018451	
	100 <i>K</i>	0.0019430	

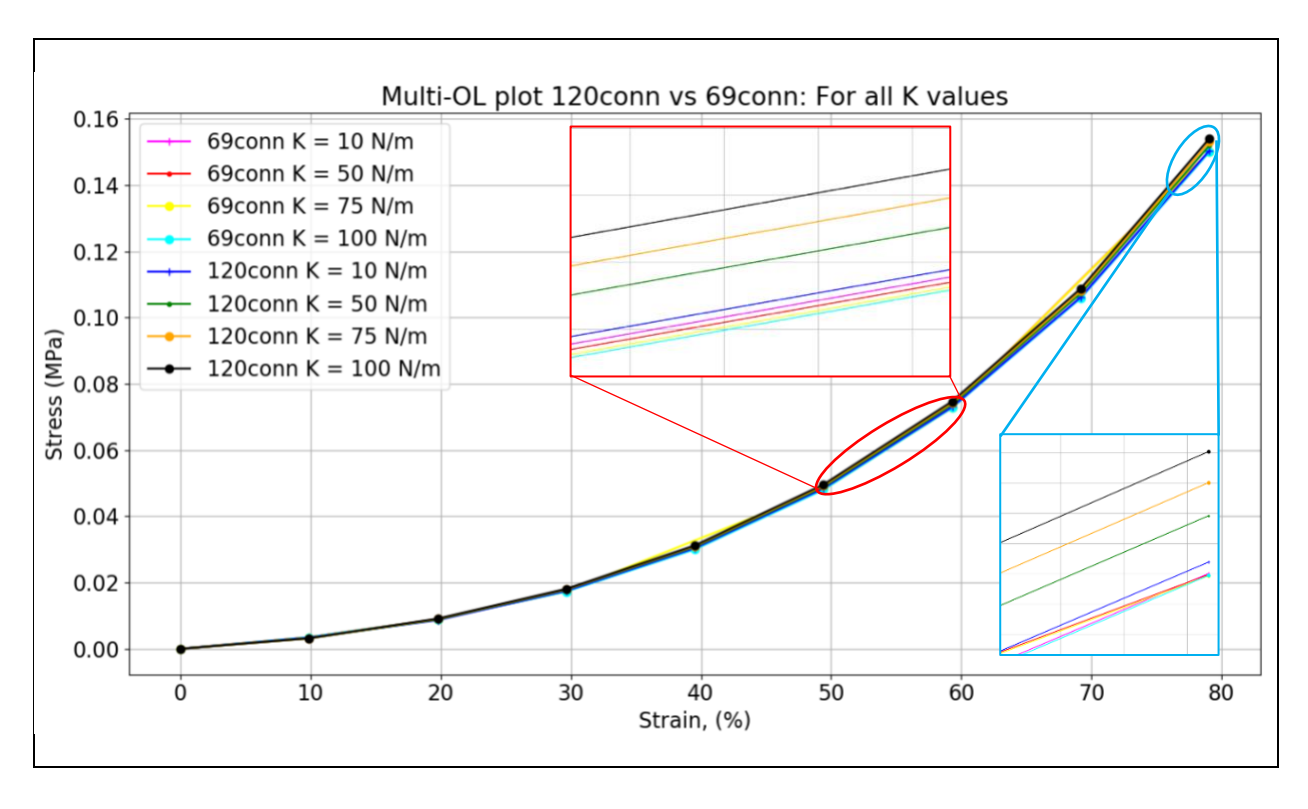


FIGURE 8: Comparison plot between original multi-OL (69 connections)[2] versus revised multi-OL model (total 120 connections) plotted. Revised multi-OL model yielded greater axonal stiffening, especially at higher K values. The two multi-OL models were compared for varying spring-dashpot stiffness value K. (Highest RMSD value between the two multi-OL variants observed to be: 0.0019430 at 100K N/m)

RMSD analysis was performed between the original multi-OL (studied in [2, 3]) and the revised multi-OL models for corresponding *K* values. It was observed that due to additional connections along the z-axis, revised multi-OL model showed greater stiffness. For brevity, original multi-OL model is denoted as 69conn_multi-OL and the revised multi-oligo model as 120conn_multi-OL. Figure 8 shows the comparative plot for the two multi-OL versions at varying *K* values. Both versions performed similarly at 10*K* (RMSD: 0.000188) but revised multi-OL model became progressively stiffer at higher *K* values (see Table 4). RMSD between the original multi-OL curve at 100*K* and the revised multi-OL curve at 10*K* was 0.000294. This indicated an appreciable increase in model sensitivity since stress in the lowest *K* configuration in revised multi-OL setup is as stiff as the 100*K* plot in the original multi-OL FE setup (Figure 8). Modifications made in multi-OL FE model addressed its geometric limitations. Greater randomization and additional connections could be incorporated to attain a stiffer mechanical response.

3.3. Single-OL model: Results and Discussion

Analyzed for varying connections

The effect of parametric change in the number of connections in single-OL model is shown in the stress-strain plot (see Figure 9) for a spring-dashpot stiffness value at K=100 N/m. Single-OL FE model plot covers five scenarios: 1, 2, 3, 4, and 5 oligodendrocyte connections per axon. Current numerical analyses consolidate the previous inferences [2, 3] by including all cases to assess single-OL model's characteristic mechanical response. There is a modest increase in axonal stiffness response with increasing connections. From Figure 9, it can be posited that for FE single-OL model, increasing tethering contributes to the greater stiffness of the axons. This is as indicated in previous research [2, 3].

Table 5: RMSD variation of single-OL FE model configurations for varying connections at 100K

RMSD Chart (single-OL) for varying connection configurations				
Nodes/ axon comparison	K value	RMSD Value		
1-node vs. 2-nodes		0.02089		
1-node vs. 3-nodes		0.02064		
2-nodes vs. 3-nodes	100 <i>K</i>	0.00041		
3-nodes vs. 5-nodes		0.00161		
4-nodes vs. 5-nodes		0.00038		

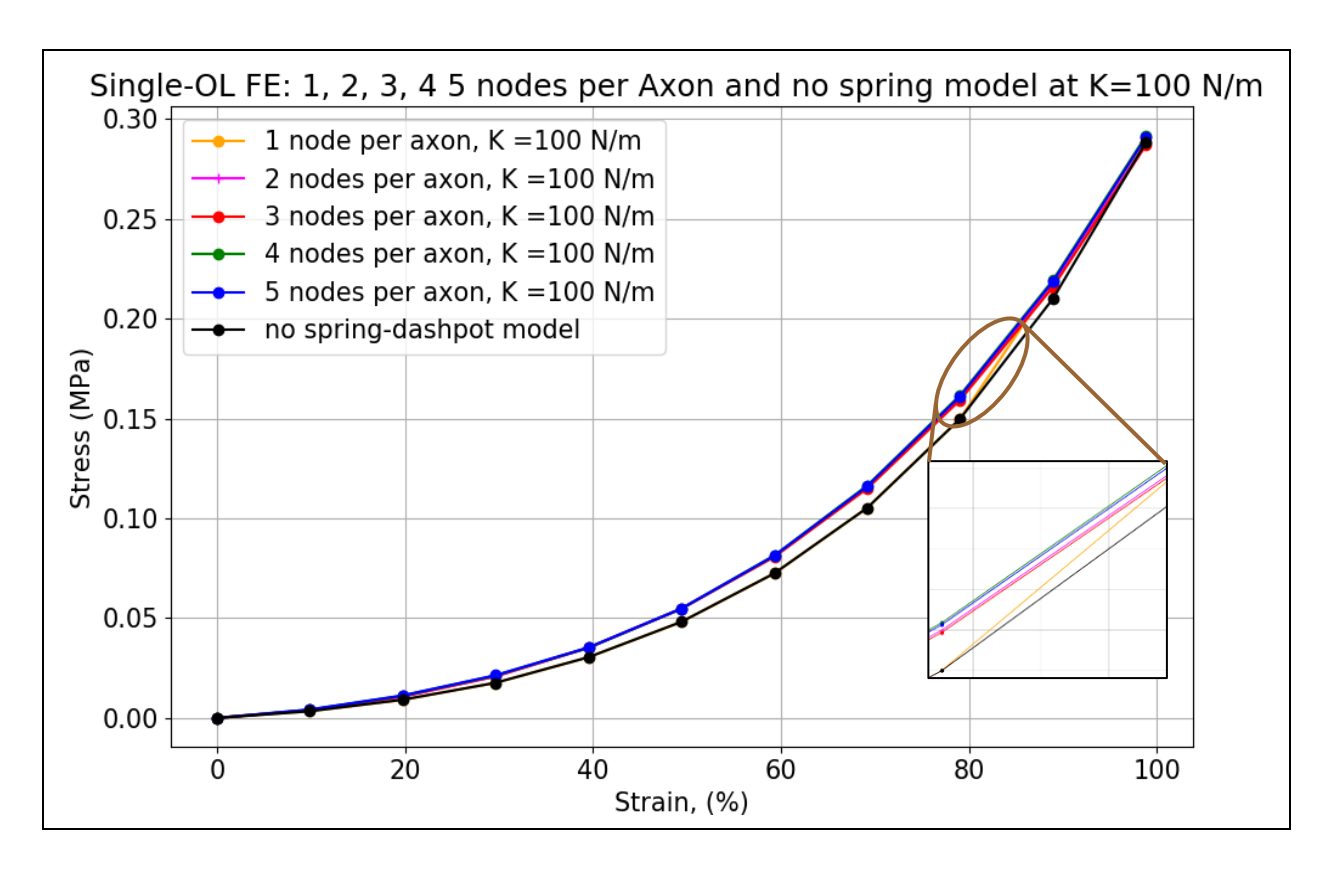


FIGURE 9: Impact of parameterization (varying connections) evaluated by overlaying 9 connections (1-node per axon), 18 connections (2-nodes per axon), 27 connections (3-nodes per axon), 36 connections (4-nodes per axon), and 45 connections (5-nodes per axon) single-OL FE results at spring-dashpot stiffness value K=100 N/m. RMSD analysis was done to quantify the relative increase in axonal stiffness.

RMSD between corresponding curves suggested minute increments, i.e., root mean square deviation (RMSD) between the 18 connections (2-nodes per axon) and 27 connections (3-nodes per axon) curves is 0.00041. For brevity, lets denote the two curves as 2-nodes vs. 3-nodes. Similar RMSD analysis for other curves revealed that differences in stress-strain response diminish as higher connection configurations are compared (see Table 5). RMSD values between curves are (4-nodes vs. 5-nodes) < (3-nodes vs. 5-nodes) < (1-node vs. 3-nodes). Higher RMSD values for 1-node vs. 2-nodes (0.02089) and 1-node vs. 3-nodes (0.02064) curves indicate the role of additional oligodendrocyte tethering in improving mechanical response, i.e., increase in stiffness. Comparison plot of the baseline FEM without tethering alongside 100K oligo-tethering models with varying connections is shown in Figure 9. RMSD value for no-spring vs 1-node curve (0.018144) clearly shows the impact due to oligo-tethering on resultant model stiffness. At very high stretch levels, the axons straighten and significantly bear the resultant stresses on the model. Hence, all models tend to converge at stretch levels close to 95-100%

Analyzed for varying "K" values

The influence of parametrization of stiffness values of oligodendrocyte arms for single-OL model is shown in Figure 10. It is seen that increasing "K" leads to a stiffer axonal response (Figure 10)

when subjected to strains of up to a maximum of 90% applied stretch. The model becomes progressively stiffer for higher values of "K". Refer to the RMSD analysis presented in Table 6.

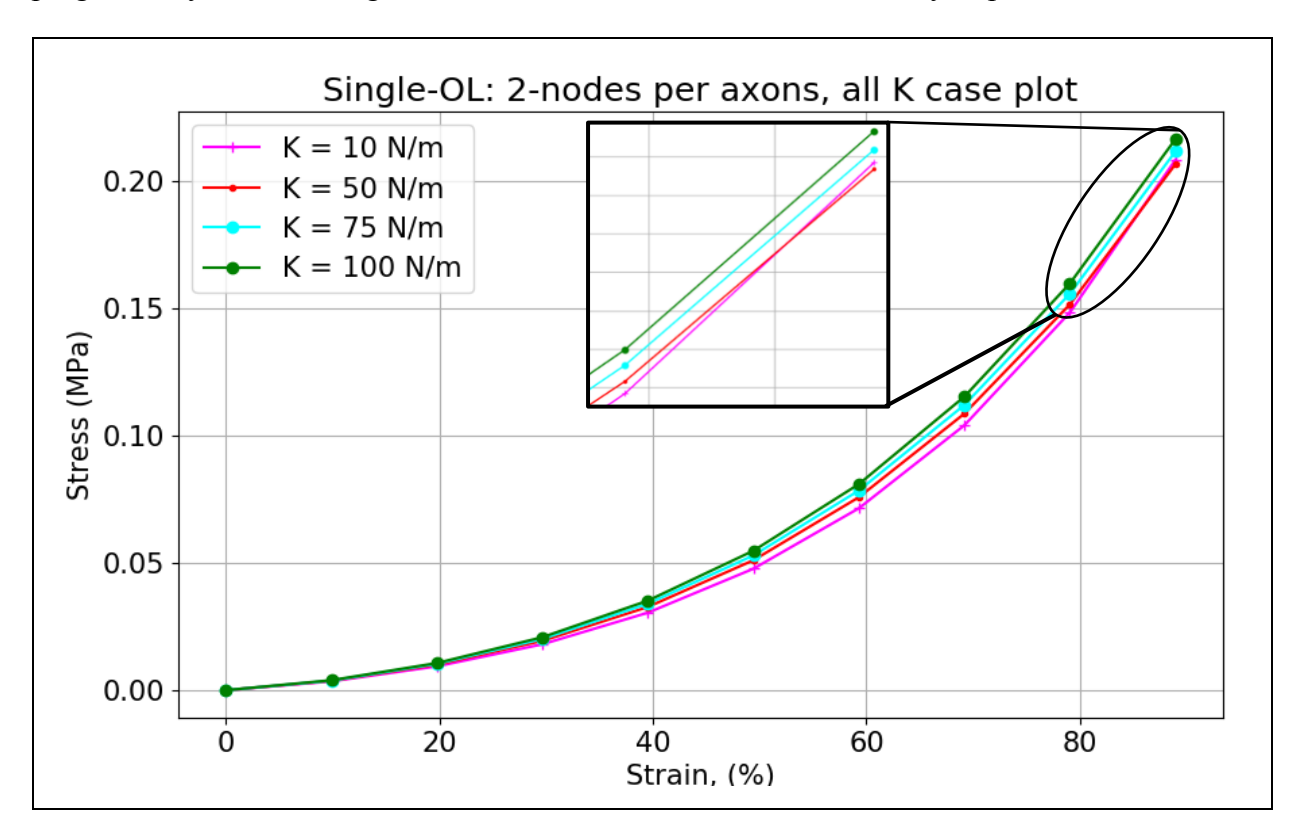


FIGURE 10: Stress-strain response for single-OL FEM parameterizing the spring-dashpot stiffness (K). Simulations performed for 2 connections per axon (total 18 connections) for K = 10, 50, 75 and 100 N/m, respectively. Trend in agreement with the stress-strain response observed for 4 and 5 oligodendrocyte connections per axon configurations [2, 3].

Results from Table 6 validate the argument that oligodendrocytes do act as a supporting scaffold for the axons in addition to the stiffening provided by the myelin sheath [2]. RMSD values tend to increase with the increasing number of connections (i.e., RMSD in 4-nodes per axon ensemble were greater than RMSD in 2-nodes per axon ensemble). Same conclusions drawn when single-OL FE model were simulated for 3-nodes, 4-nodes, and 5-nodes per axon tethering cases.

Table 6: RMSD variations for varying K values in single-OL model for 2-nodes per axon case

RMSD Variation (single-OL: 2 nodes per axon case) for varying K values			
Plots compared	RMSD Value		
10 <i>K</i> and 50 <i>K</i>	0.002666		
10 <i>K</i> and 75 <i>K</i>	0.004720		
10K and 100K	0.007035		

3.4. Multi-OL vs. single-OL: Results and Discussion

The micromechanical FE models generate similar stress-strain profiles, although some contrasting results have been observed in relative stiffness in response to tensile loads in current and previous studies [2, 3]. In one of our previous studies, multi-OL models proved slightly stiffer than the single-OL model. However, in the next installment of our research, 4-node per axon (36 connections) FE model with K = 100 N/m revealed that the single-OL FE model is stiffer than the multi-OL model (see Figure 10 [3] and Figure 12 in this paper). In this current research, geometrical limitations in the multi-OL FE model have been mitigated to a significant extent by introducing additional connections (see §3.2), and this is reflected by the RMSD value (0.004941) between the two plots (Figure 12).

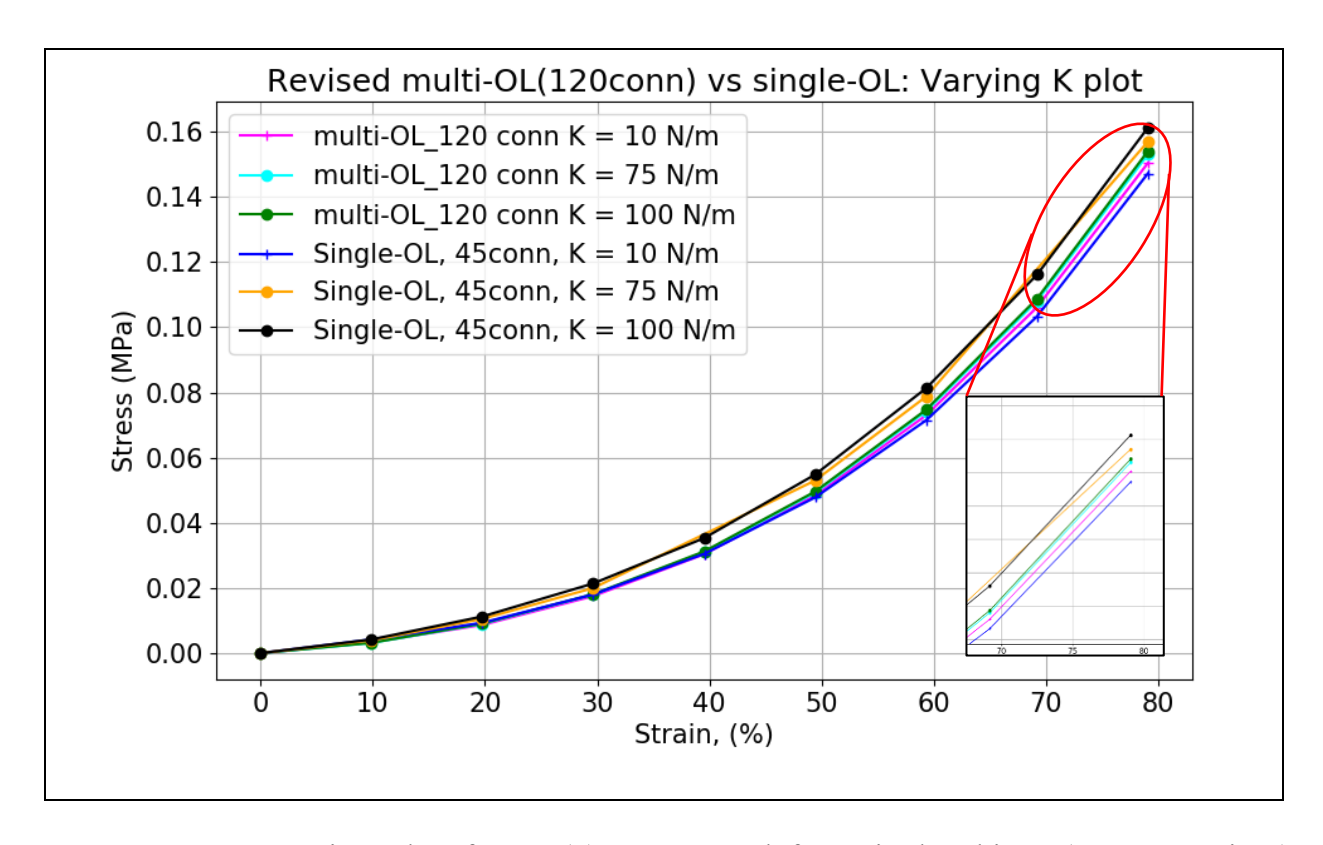


FIGURE 11: Comparison plot of stress (σ) versus stretch for revised multi-OL (120 connections) and single-OL plotted for varying spring-dashpot stiffness (K) up to 80% strain. Multi-OL model-showed marginal mechanical response variation with varying K. Single-OL FE model proved to be stiffer at higher K values.

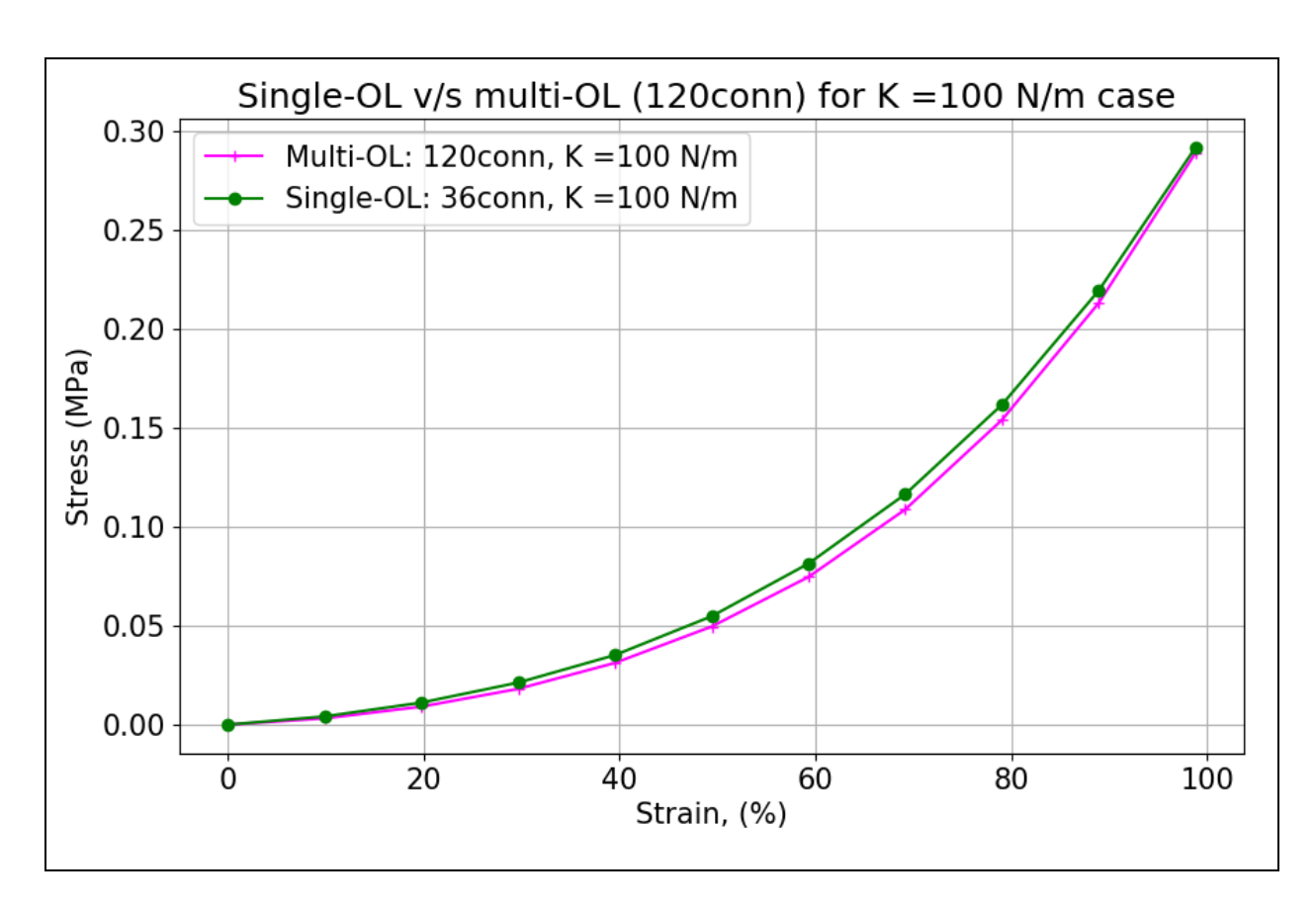


FIGURE 12: Revised multi-OL (120 connections) versus single-OL (total 36 connections) plotted, and single-OL found to yield greater axonal stiffening. The two models were compared with a constant spring-dashpot stiffness value K = 100 N/m. (RMSD value: 0.004941)

Table 7: Comparison of single-OL FEM with variants of multi-OL FE models at 80% stretch

Compared multi-OL vs. single-OL @ K = 100 N/m	RMSD multi-OL (69 conn) vs. single-OL	RMSD Revised multi-OL (120 conn) vs. single- OL	% Change in RMSD	Comment on relative model stiffness comparison
SM 1 vs. 9 conn SM2	0.000311	0.002051	559.48%	SM1(120) > SM2
SM 1 vs. 18conn SM2	0.006218	0.004367	29.77%	SM2 > SM1
SM 1 vs. 27conn SM2	0.005982	0.004147	30.68%	SM2 > SM1
SM 1 vs. 36conn SM2	0.006846	0.004965	27.48%	SM2 > SM1
SM 1 vs. 45conn SM2	0.006693	0.004824	27.92%	SM2 > SM1

Note: abbreviations SM1 refers to multi-OL (submodel-1[2]: multi-oligo) FEM and SM2 means single-OL (submodel-2[2]: single oligo) FEM. SM1(120) refers to the revised multi-OL FEM.

Due to modifications in multi-OL FEM, stiffness improved significantly. For instance, revised multi-OL was observed to be way stiffer than 1-node per axon single-OL case (i.e., 120conn multi-OL >> 9conn_single-OL). In contrast, the same comparison analysis between original multi-OL vs. single-OL showed similar performance (RMSD: 0.000311). For the remaining cases in the ensemble, although single-OL exhibits dominant mechanical response, RMSD values between the revised multi-OL and single-OL curves have decreased (see Table 7). Exhaustive RMSD comparison analysis was conducted for the remaining cases in the ensemble (such as 18 conn, 27 conn 36 conn, and 45 conn) at K = 100 N/m. Since in single-OL FEM, an oligodendrocyte is positioned at the center, and each spring-dashpot connection is subjected to a relatively greater stretch when compared to multi-OL. Hence, greater axonal stiffness was recorded for single-OL when compared against each multi-OL FEM at K = 100 N/m for varying connections (Table 7).

4. Model Limitations and Outlook

The proposed FE model has potential limitations. Firstly, non-affine boundary conditions have been approximated for the entire stretch history even though axons tend to exhibit more transitional behavior physiologically. Future FE model versions which incorporate transition mechanisms could deliver high fidelity results [11]. The proposed model approximates oligodendrocyte-axonal tethering via linear spring-dashpot connections. Revised multi-OL FEM compared closely to single-OL FEM at higher *K* values (see Figure 11), thus corroborating the improvement in performance of revised multi-OL. It is conjectured that greater randomization in inter-planar connections could further improve mechanical response in multi-OL. Lastly, damage initiation and evolution mechanics could be incorporated in future simulations.

Physiologically it is firmly established that oligodendrocytes support axons by covering them with a sheath of myelin, but their tethering to axons also plays a crucial role in improving axonal stiffness. While the proposed FE model has scope for further refinement, it serves as proof-of-concept to understand the mechanical response in axons and ECMs. In future, the FE models can be tailored to incorporate a range of mechanical properties for axons and ECM and examine transitional behavioral mechanisms (affine to non-affine boundary conditions) to generate high fidelity results [2, 3]. Next, oligodendrocyte-axonal tethering could be modeled with non-linear spring-dashpot connections. The current hyperelastic constitutive model can be adjusted to incorporate the impact of variations in ' α ' and study corresponding nonlinearity introduced by it. As a future research objective, current FE submodels are also being improved to conduct aging brain analysis [3, 50, 51]. Further research is being carried out to parametrically determine the influence of changing constitutive material model parameters to determine an aging brain matter's mechanical response [3] and determine higher-order tissue decay/softening characteristics.

As an extension to the current study, an elaborated FE model setup incorporating non-linear connection types and material parameters could help probe the causes behind damage initiation and evolution mechanics in healthy and aging brain matter [3]. Such an exhaustive FE setup would facilitate the depiction of repair and recovery mechanisms in brain tissues. Bending stresses undergoing cyclic reversal were found prominent in undulating axons. Formulating a 3D FE model incorporating damage accumulation from repeated loading would provide a thorough intuition of structural response in young, aging, or injured axons against external loads.

5. Conclusions

A novel 3D simulation framework comprising two FE submodels, namely the multi-OL and the single-OL FEM have been investigated. In the multi-OL FE setup, multiple oligodendrocytes arbitrarily tethered to the nearest axons, whereas, in the single-OL FEM, a single oligodendrocyte stationed centrally tethered to all axons at various locations. The proposed FEM depict mechanical response variation in white matter using purely non-affine boundary conditions. This proof-of-concept model helped numerically represent connections mechanism in white matter between the oligodendrocytes and axons. The developed FEM thereby served to probe the effect of oligodendrocytes tethering and depict axonal mechanical response.

The model has the potential to estimate the extent of axonal injuries, given that the threshold values of the axonal damage are established. Since the proposed 3D FEM incorporates undulations in axonal geometry, it can depict the cyclic reversal in bending stresses experienced along their tortuous path. Thus, the discussed FE models might serve as the foundation for future research on axonal repeated load and trauma due to damage accumulation. To the authors' knowledge, this is the first time that computational embodiment of variable stiffness oligodendrocyte connections using non-affine kinematics has revealed localized stress reversal.

To comprehensively understand the axonal stiffness response, an ensemble of simulation scenarios has been analyzed using two proposed FE submodels (multi-OL and single-OL FEM). Corroborating with our previous data, the new batch of results indicates the appearance of bending stresses along their tortuous path [2, 3] with stress reversal. These bending stresses render the axons susceptible to repeated load failure. While diffuse axonal injuries could destroy axons in a very short time (within milliseconds), repeated stresses may need multiple cycles before causing failure. Hyperelastic materials also suffer from damage caused by low and high fatigue loads [49]. From the brain white matter context, the magnitude of bending stresses largely depends on the axons' random geometry. In both discussed submodels, resultant bending stress magnitude or pertinent cerebral damage is seen to be dependent on axonal geometry, brain mass variations, loading direction, and current state of the shear moduli (impact of aging, injury, or atrophy) [52]. Further research incorporating damage models for the axons subjected to cyclic loads is required to truly understand axonal damage and trauma due to damage accumulation from repeated impact to the brain [2].

Parametrizing oligodendrocyte connections for the tested ensemble of cases in both FE submodels indicates that axonal stiffness increases with increasing connections. Along with increasing oligodendrocyte-axon tethering connections, greater oligodendrocyte arm stiffness "K-value" further improves its stiffening response. As conjectured in the previous studies, this trend could be attributed to the recruitment of nodes of Ranvier, which causes this increment [2]. Thus, oligodendrocyte connections are pivotal in improving stress-strain response to an external load. While oligodendrocytes support the axons by creating a sheath of myelin around them, this study, also suggests the possibility of a direct influence on the axons' mechanical response due to oligodendrocytes tethering. Thus, proposed FE model fittingly served as proof-of-concept to understand mechanical response in axons and ECMs. To end, more intricate FEM setup incorporating damage initiation, evolution, and accumulation behavior could be developed to gain in-depth understanding on young, aging, or injured axons' structural response.

Acknowledgments

The authors gratefully acknowledge the support provided by NSF Grant CMMI-1763005 and the program director Dr. Laurel Kuxhaus.

References

- 1. Capizzi, A., J. Woo, and M. Verduzco-Gutierrez, *Traumatic Brain Injury: An Overview of Epidemiology, Pathophysiology, and Medical Management.* The Medical clinics of North America, 2020. **104**(2): p. 213-238.
- 2. Pasupathy, P., R. De Simone, and A.A. Pelegri. *Numerical Simulation of Stress States in White Matter via a Continuum Model of 3D Axons Tethered to Glia*. in *ASME 2020 International Mechanical Engineering Congress and Exposition*. 2020. Portland, OR, USA: ASME.
- 3. Agarwal, M., et al. Oligodendrocyte Tethering Effect on Hyperelastic 3D Response of Injured Axons in Brain White Matter. in ASME 2021 International Mechanical Engineering Congress and Exposition. 2021.
- 4. Thurman, D.J., Traumatic brain injury in the United States; a report to Congress. 1999.
- 5. Ratajczak, M., et al., *Material and structural modeling aspects of brain tissue deformation under dynamic loads.* Materials, 2019. **12**(2): p. 271.
- 6. Langlois, J.A., W. Rutland-Brown, and M.M. Wald, *The epidemiology and impact of traumatic brain injury: a brief overview.* The Journal of head trauma rehabilitation, 2006. **21**(5): p. 375-378.
- 7. Arbogast, K.B. and S.S. Margulies, *Material characterization of the brainstem from oscillatory shear tests.* Journal of Biomechanics, 1998. **31**(9): p. 801-807.
- 8. Bain, A.C. and D.F. Meaney, *Tissue-level thresholds for axonal damage in an experimental model of central nervous system white matter injury*. Journal of biomechanical engineering, 2000. **122**(6): p. 615-622.
- 9. Cloots, R., et al., *Biomechanics of traumatic brain injury: influences of the morphologic heterogeneities of the cerebral cortex.* Annals of biomedical engineering, 2008. **36**(7): p. 1203-1215.
- 10. Cloots, R., et al., *Micromechanics of diffuse axonal injury: influence of axonal orientation and anisotropy.* Biomechanics modeling in mechanobiology, 2011. **10**(3): p. 413-422.
- 11. Pan, Y., et al., Finite element modeling of CNS white matter kinematics: use of a 3D RVE to determine material properties. Frontiers in bioengineering biotechnology, 2013. 1: p. 19.
- 12. Singh, S., A.A. Pelegri, and D.I. Shreiber, *Characterization of the three-dimensional kinematic behavior of axons in central nervous system white matter.* Biomechanics modeling in mechanobiology, 2015. **14**(6): p. 1303-1315.
- 13. Pan, Y., D.I. Shreiber, and A.A. Pelegri, *A transition model for finite element simulation of kinematics of central nervous system white matter.* IEEE transactions on biomedical engineering, 2011. **58**(12): p. 3443-3446.
- 14. Yousefsani, S.A., A. Shamloo, and F. Farahmand, *Micromechanics of brain white matter tissue:* a fiber-reinforced hyperelastic model using embedded element technique. Journal of the mechanical behavior of biomedical materials, 2018. **80**: p. 194-202.

- 15. Karami, G., et al., A micromechanical hyperelastic modeling of brain white matter under large deformation. Journal of the mechanical behavior of biomedical materials, 2009. **2**(3): p. 243-254.
- 16. Hao, H. and D. Shreiber, *Axon kinematics change during growth and development.* Journal of biomechanical engineering, 2007. **129**(4): p. 511-522.
- 17. Shreiber, D.I., H. Hao, and R.A. Elias, *Probing the influence of myelin and glia on the tensile properties of the spinal cord*. Biomechanics modeling in mechanobiology, 2009. **8**(4): p. 311-321.
- 18. Allen, N.J. and B.A. Barres, *Glia—more than just brain glue*. Nature, 2009. **457**(7230): p. 675-677.
- 19. Simons, M. and K.-A. Nave, *Oligodendrocytes: myelination and axonal support*. Cold Spring Harbor perspectives in biology, 2016. **8**(1): p. a020479.
- 20. Gennarelli, T.A., *Mechanisms and pathophysiology of cerebral concussion*. The Journal of Head Trauma Rehabilitation, 1986. **1**(2): p. 23-29.
- 21. Margulies, S.S., L.E. Thibault, and T.A. Gennarelli, *Physical model simulations of brain injury in the primate.* Journal of biomechanics, 1990. **23**(8): p. 823-836.
- 22. Arbogast, K., S. Margulies, and L. Thibault, *Strain in the brainstem during rotational head injury*. ASME-PUBLICATIONS-BED, 1994. **28**: p. 315-315.
- 23. Brooks, T., et al., Finite element models and material data for analysis of infant head impacts. Heliyon, 2018. **4**(12): p. e01010.
- 24. Ruan, J.S., T.B. Khalil, and A.I. King, *Finite element modeling of direct head impact*. 1993, SAE Technical Paper.
- 25. Zhou, C., T.B. Khalil, and A.I. King, *A new model comparing impact responses of the homogeneous and inhomogeneous human brain.* SAE transactions, 1995: p. 2999-3015.
- 26. Kang, H.-S., et al., Validation of a 3D anatomic human head model and replication of head impact in motorcycle accident by finite element modeling. SAE transactions, 1997: p. 3849-3858.
- 27. Margulies, S.S. and K.L. Thibault, *Infant skull and suture properties: measurements and implications for mechanisms of pediatric brain injury.* Journal of biomechanical engineering, 2000. **122**(4): p. 364-371.
- 28. Li, Z., et al., Development, validation, and application of a parametric pediatric head finite element model for impact simulations. Annals of biomedical engineering, 2011. **39**(12): p. 2984-2997.
- 29. Montanino, A., et al., Subject-specific multiscale analysis of concussion: from macroscopic loads to molecular-level damage. Brain multiphysics, 2021. **2**: p. 100027.
- 30. Montanino, A., et al., Axons embedded in a tissue may withstand larger deformations than isolated axons before mechanoporation occurs. Journal of biomechanical engineering, 2019. **141**(12).
- 31. Montanino, A. and S. Kleiven, *Utilizing a structural mechanics approach to assess the primary effects of injury loads onto the axon and its components.* J Frontiers in neurology, 2018: p. 643.
- 32. Li, X., H. Sandler, and S. Kleiven, *The importance of nonlinear tissue modelling in finite element simulations of infant head impacts.* Biomechanics modeling in mechanobiology, 2017. **16**(3): p. 823-840.

- 33. Thibault, K.L. and S.S. Margulies, *Age-dependent material properties of the porcine cerebrum:* effect on pediatric inertial head injury criteria. Journal of biomechanics, 1998. **31**(12): p. 1119-1126.
- 34. Coats, B. and S.S. Margulies, *Material properties of human infant skull and suture at high rates*. J Journal of neurotrauma, 2006. **23**(8): p. 1222-1232.
- 35. Meaney, D.F., Relationship between structural modeling and hyperelastic material behavior: application to CNS white matter. Biomechanics modeling in mechanobiology, 2003. **1**(4): p. 279-293.
- 36. Naik, A., et al., *Micromechanical viscoelastic characterization of fibrous composites*. Journal of composite materials, 2008. **42**(12): p. 1179-1204.
- 37. Coats, B., S.S. Margulies, and S. Ji, *Parametric study of head impact in the infant.* Stapp Car Crash J, 2007. **51**(1-15).
- 38. Abolfathi, N., et al., A micromechanical procedure for modelling the anisotropic mechanical properties of brain white matter. Computer Methods in Biomechanics Biomedical Engineering, 2009. **12**(3): p. 249-262.
- 39. Javid, S., A. Rezaei, and G. Karami, *A micromechanical procedure for viscoelastic characterization of the axons and ECM of the brainstem.* Journal of the mechanical behavior of biomedical materials, 2014. **30**: p. 290-299.
- 40. de Simone, R., Direct Numerical Simulation of Stress States in White Matter via a Triphasic Continuum Model of 3D Axons Tethered to Glia. 2019, Rutgers The State University of New Jersey, School of Graduate Studies.
- 41. Abaqus, U.m.M., Standard, Hibbitt, Karlsson, and Sorensen. 2005.
- 42. Singh, S., A.A. Pelegri, and D.I. Shreiber, *Estimating axonal strain and failure following white matter stretch using contactin-associated protein as a fiduciary marker*. Journal of biomechanics, 2017. **51**: p. 32-41.
- 43. Wu, X., J.G. Georgiadis, and A.A. Pelegri. *Biphasic Representative Elemental Volumes for 3-D White Matter Elastography*. in *ASME International Mechanical Engineering Congress and Exposition*. 2021. American Society of Mechanical Engineers.
- 44. Mihai, L.A., et al., *A family of hyperelastic models for human brain tissue*. Journal of the Mechanics and Physics of Solids, 2017. **106**: p. 60-79.
- 45. Dill, E.H., *The finite element method for mechanics of solids with ANSYS applications*. Vol. 6000. 2012: CRC press New York.
- 46. Wu, X., J.G. Georgiadis, and A.A. Pelegri. *Brain White Matter Model of Orthotropic Viscoelastic Properties in Frequency Domain*. in *ASME International Mechanical Engineering Congress and Exposition*. 2019. American Society of Mechanical Engineers.
- 47. Bain, A.C., D.I. Shreiber, and D.F. Meaney, *Modeling of microstructural kinematics during simple elongation of central nervous system tissue.* Journal of biomechanical engineering, 2003. **125**(6): p. 798-804.
- 48. Verron, E., G. Chagnon, and J.-B. Le Cam, *Hyperelasticity with volumetric damage*. Constitutive models for rubber VI. Rotterdam, The Netherlands: Balkema, 2010: p. 279-284.
- 49. Ayoub, G., et al., Modeling the low-cycle fatigue behavior of visco-hyperelastic elastomeric materials using a new network alteration theory: Application to styrene-butadiene rubber. Journal of the Mechanics and Physics of Solids, 2011. **59**(2): p. 473-495.

- 50. Sack, I., et al., *The impact of aging and gender on brain viscoelasticity.* Neuroimage, 2009. **46**(3): p. 652-657.
- 51. Sack, I., et al., The influence of physiological aging and atrophy on brain viscoelastic properties in humans. PloS one, 2011. **6**(9): p. e23451.
- 52. Kleiven, S., Evaluation of head injury criteria using a finite element model validated against experiments on localized brain motion, intracerebral acceleration, and intracranial pressure. International Journal of Crashworthiness, 2006. **11**(1): p. 65-79.
- 53. Budday, S., et al., *Fifty shades of brain: a review on the mechanical testing and modeling of brain tissue*. Archives of Computational Methods in Engineering, 2019. **27**: p. 1187–1230.

APPENDIX A

Hyperelastic Material (H-E) model & material property definition details

Non-linear hyperelastic models are commonly used to simulate soft biological tissues [11, 13, 23, 35]. Some of the pioneering work in the field include Ogden hyperelastic material model from Pan et al. [11-13] who simulated kinematics of CNS white matter, Karami et al. [15] who introduced the embedded element approach and Mihai et al. [44] utilized experimental results to formulate hyperelastic material models. Several hyperelastic material models have been studied recently, such as Mooney-Rivlin [23], neo-Hookean, Demiray, Gent, and modified Ogden models [53]. This paper utilizes the Ogden hyperelastic material model to simulate the ECM and the axons [2]. The non-linearity of the Ogden model allows neural tissue to be characterized more accurately for large deformation and strains. The Ogden hyperelastic model is based on the three principal stretches λ_1 , λ_2 , λ_3 , and 2N material constants. The strain energy density function, W, for the Ogden material model (Equation A.1) in Abaqus is formulated as [2, 41]:

$$W = \sum_{1}^{N} \frac{2\mu_{i}}{\alpha_{i}^{2}} \left(\lambda_{1}^{-\alpha_{i}} + \lambda_{2}^{-\alpha_{i}} + \lambda_{3}^{-\alpha_{i}} - 3 \right) + \sum_{1}^{N} \frac{1}{D_{i}} (J_{el} - 1)^{2i}$$
 (A.1)

where $\overline{\lambda_i} = J_{el}^{-\frac{1}{3}} \lambda_i$ and $\overline{\lambda_1 \lambda_2 \lambda_3} = 1$. μ_i represents shear moduli, while α_i and D_i are material parameters. The first and second terms represent the strain energy function's deviatoric and hydrostatic components. The parameter $D_i = \frac{2}{K_0}$, allows for the inclusion of compressibility where K_0 is the initial bulk modulus. An incompressible, single parameter Ogden hyperelastic material is considered in this study. Therefore, N = 1. Incompressibility implies that $J_{el} = 1$ and is specified in Abaqus by setting $D_1 = 0$. As a result, Abaqus eliminates the hydrostatic component of the strain energy density equation, and the expression reduces (Equation A.2)

$$W = \sum_{1}^{N} \frac{2\mu_{i}}{\alpha_{i}^{2}} \left(\lambda_{1}^{-\alpha_{i}} + \lambda_{2}^{-\alpha_{i}} + \lambda_{3}^{-\alpha_{i}} - 3 \right)$$
 (A.2)

The corresponding principal stress is expressed as (Equation A.3):

$$\sigma_{uniaxial} = \frac{2\mu}{\alpha} \left[\lambda^{\alpha} - \left(\frac{1}{\sqrt{\lambda}} \right)^{\alpha} \right] \tag{A.3}$$

Undulation prevents axons from experiencing full tension until the axon is straightened and the tortuosity becomes 1. In this study, the values for shear modulus for the axons and ECM are obtained from research by Wu et al. [46] while α is derived from the model developed by Meaney [35]. The shear modulus of the ECM is assigned relative to the shear modulus of the axon,

considering axons are three times stiffer than ECM, as reported by Arbogast and Margulies [7]. Three coefficients needed to be used for the axons and ECM: Shear modulus (μ_i), nonlinear parameter (α_i), and compressibility factor (D_i). As mentioned above, the values for shear modulus and the nonlinear parameter were provided by test data presented in Meaney's research [35]. The shear modulus of the ECM is derived from the shear modulus assigned to the axon, as the axon is three times stiffer than the ECM per Arbogast and Margulies's findings [7]. Therefore, the shear modulus of the ECM, is the value of the axon shear modulus divided by a factor of three. To remain consistent with works previously performed, the nonlinear parameter assigned to the axons and ECM are given the same value. Axons and ECM are assumed incompressible [40] and therefore D is set to zero. The oligodendrocyte material properties for the generalized hyper-elastic Ogden model are $\mu_0 = 32.8 \text{ kPa}$, $\alpha = 8.22 \text{ [17]}$.